行政院國家科學委員會專題研究計畫　成果報告

側向開口端部封閉管流紊流器熱傳及流場效應探討

計畫類別：個別型計畫
計畫編號：NSC94-2212-E-032-009-
執行期間：94 年 08 月 01 日至 95 年 07 月 31 日
執行單位：淡江大學航空太空工程學系

計畫主持人：陳增源

報告類型：精簡報告

處理方式：本計畫可公開查詢

中　華　民　國 95 年 11 月 7 日

行政院國家科學委員會補助專題研究計畫 ■ 成 果 報 告
□期中進度報告

側向開口端部封閉管流
紊流器熱傳及流場效應探討

計畫類別：■ 個別型計畫　　□ 整合型計畫
計畫編號：NSC 94－2212－E－032－009－
執行期間：　94 年　08 月　01 日至　95 年　07 月　31 日

計畫主持人：陳增源
共同主持人：
計畫參與人員：

成果報告類型(依經費核定清單規定繳交)：■精簡報告　□完整報告

本成果報告包括以下應繳交之附件：
□赴國外出差或研習心得報告一份
□赴大陸地區出差或研習心得報告一份
□出席國際學術會議心得報告及發表之論文各一份
□國際合作研究計畫國外研究報告書一份

處理方式：除產學合作研究計畫、提升產業技術及人才培育研究計畫、列管計畫及下列情形者外，得立即公開查詢
□涉及專利或其他智慧財產權，□一年□二年後可公開查詢

執行單位：淡江大學航太系

中　華　民　國　　95　年　　10　月　　30　日

Abstract

Flow characteristics and heat transfer in side-opened, end-sealed duct flows without and with a 45° delta-wing turbulator were experimentally investigated. Three-component mean and fluctuating velocity measurements were conducted at duct cross-sections and near duct wall by a laser Doppler velocimetry to characterize flow structures and to obtain near-wall flow parameters, including the convective mean velocity, second-flow velocity and turbulent kinetic energy. A heated copper plate, installed on the duct bottom wall, was used as a heat transfer surface. Temperatures on the heat transfer surface were measured using thermocouples to obtain the local and averaged Nusselt numbers. The investigated Reynolds numbers were between 1546 and 15151. Results of this study show that the flow reversal, recirculation, reattachment and redevelopment occur in the investigated duct flows. Also, the flows exhibit free and retarded stagnation point flow behaviors. The turbulator causes large regions of small convective mean velocity, and, in general, increases the flow secondary-flow and turbulence effects. Results also show that the turbulator augments the heat transfer rate, which is mainly caused by the increases of the flow secondary-flow and, especially, the turbulence effects. The heat transfer augmentation increases with Reynolds number. The local heat transfer distributions for Reynolds numbers of 1546 and 15151 are dominated by the flow convective mean velocity and turbulent kinetic energy, respectively.
Keywords: side-opened end-sealed duct flow, heat transfer, turbulator

摘要

本研究利用側向開口端部封閉管道，實驗探討 45° 三角翼紊流產生器之流場及熱傳效應。研究內容主要包括利用雷射設測速移做不同斷面及近壁面三維平均及擾動速度量測，探討紊流產生器對流場結構及邊界層內流場對流、二次流及紊流特性影響；一加熱銅板置於管道底部作為熱傳面，利用熱電偶作溫度量測，探討局部及平均熱傳分佈；流場雷諾數介於 1546 至 15151。研究結果顯示，在探討管流中，流場產生逆向流、迴流、再接觸及再發展之流場特性，同時流場有自由停滯及般延遲停滯流特性；45° 三角翼紊流產生器之影響，造成更大區域之逆向流以及較大區域之”死水區”，因而有較差之流場對流效應，但一般而言，有較佳之二次流效應及紊流效應。局部熱傳之分佈在 Re=1546 時係由對流平均速度分佈來主導，而在 RE=15151 時係由紊流動能分佈主導，

關鍵字：紊流產生器、側向開口端部封閉管流、熱傳

1. Introduction

Heat sinks play an important role in the heat dissipation in electronics, heat exchangers, computers and so on. To cope with the ever mounting cooling duty of heat sinks, extensive studies have been conducted on heat transfer augmentation by various types of turbulators, including rib turbulators, arrays of pin fins, wing-type turbulators, shaped roughness elements, arrays of dimples and so on. For example, Eibeck and Eaton [1] experimentally examined the heat transfer effects of an isolated longitudinal vortex embedded in a turbulent boundary layer. They found that the longitudinal vortex effects on the Stanton number were attributed largely to the distortion in the mean velocity field. Fiebig and his group [2-4] conducted systematic experimental investigations on heat transfer enhancement and induced drag using delta wings, rectangular wings, delta winglets and rectangular winglets in channel uniform flows. They found that the heat transfer was increased up to 60^o angle of attack. The heat transfer enhancement per unit vortex generator area was the highest for delta wings followed by delta winglets and rectangular winglets [2]. Their studies also showed that the vortices in the wake of the second row were more unsteadiness than the first-row vortices [3]. A pair of delta winglets performed slightly better than a pair of rectangular winglets at higher angles of attack and Reynolds numbers [4]. Tsai and Hwang [5] and Liou et al. [6] investigated the effects of ridge shapes and rib-arrays on heat transfer. Their studies showed that various ridge shapes have comparable thermal performance and the composite-ribbed performed best in their ribbed configurations. Liou et al. [7] also studied the effect of divider thickness on the local heat transfer distributions. Their results showed that the direction and strength of the secondary flow are the most important fluid dynamic factors affecting the heat transfer distributions, followed by the convective mean velocity and then the turbulent kinetic energy. Chen et al. [8-9] experimentally investigated wing-type turbulator effects on flow characteristics and heat transfer in duct fan flows. Their studies indicate that the rectangular- and delta-wing turbulators are able to augment heat transfer. The augmentation by the rectangular-wing turbulator in fan flows is as effective as in uniform flows [8]. However, the delta-wing effect on heat transfer in fan flows is not as attractive as in uniform flows [9].

The previous studies focused on the investigations of turbulator effects on heat transfer and flow characteristics in general duct flows and fan flows, and indicated that turbulators have substantial effects on heat transfer rates. In many fin-array heat sinks, the air streams flow in side-opened, end-sealed ducts, where the air continuously leaks from two side openings prior to impinging on the ends of ducts. The heat transfer and flow characteristics in such duct flows should apparently be different those in general duct flows and fan flows, and such studies have less been seen in the literature. Recently, Chang et al. [10] investigated the heat transfer in three side-opened and bottom sealed channels with two opposite walls roughened by 90^o staggered ribs. Results of their study show that the augmentation of spatially averaged heat transfer by the 90^o staggered ribs is in the range of 140-200% of the flat fins. They also formulated a criterion for selecting the optimal length-to-gap ratio of a fin channel, which provides the maximum convective heat flux from the rib-roughened fin surface. Chiang et al. [11] also investigated the heat transfer in three side-opened and bottom sealed channels with two opposite walls roughened by 45^o staggered ribs. Results show that the 45^o staggered ribs could further enhance heat transfer by 10-50% over the 90^o staggered ribs. These studies mainly focused on the heat transfer, but the flow characteristics were less addressed. Also, the relations between the flow characteristics and heat transfer were not discussed in these researches. The present study first investigates the cross-sectional flow structures in side-opened, end-sealed duct flows without and with a 45^o delta-wing turbulator. Three near-wall flow parameters, including the convective mean velocity, secondary-flow velocity and turbulent kinetic energy are then obtained from the measured three-component mean and fluctuating velocities. Temperature distributions on a heat transfer surface are measured to obtain local and averaged Nusselt numbers. Relations between the near-wall flow characteristics and local Nusselt number distributions are discussed. The turbulator effects on flow characteristics and heat transfer are addressed.

2. Experimental setup and methods

The primary experimental setup utilized in this research is shown in Fig. 1. An open-circuit wind tunnel system, including a frequency controller, a blower, a diffuser, honeycombs, screens and a contraction section, was used to develop uniform air flows with turbulence intensities less than 0.5 percent at the inlet of a 12 x 3 cm^2, 9 *cm* long test duct. The side walls of test duct were removed, and the end of test duct was sealed. The air continuously flows out from two side openings prior to impinging on the end of duct. A 45^o delta-wing turbulator may be placed on the bottom wall, 2.75 *cm* upstream of the test duct. The base width and tip height of the turbulator are 12 *cm* and 0.7 *cm*, respectively. The bottom wall of test duct is served as the heat transfer surface. The duct average velocities were between 0.51 *m/s* and 5 *m/s*, where the corresponding Reynolds numbers are between 1546 and 15151 based on the duct hydraulic diameter.

Three-component, mean and fluctuating velocity measurements were performed using a TSI laser Doppler velocimetry (LDV). Each velocity is calculated from 8192 collected velocity samples. The local

mean velocity ($\bar{v}$) is the average value of the 8192 velocity samples and the fluctuating velocity is obtained from $\sqrt{\sum v^2/8192-\bar{v}^2}$, where v is the local instant velocity. A smoke generator was used to generate smoke particles, which were sucked into the test duct by the blower, for the LDV measurements. These measurements were conducted at duct X-Y and X-Z planes to characterize the flow structures, and 2 *mm* from the heat transfer surface to obtain near-wall flow parameters, including the convective mean velocity, secondary-flow velocity and turbulent kinetic energy. The uncertainty in the measured velocity ranges was less than 5 percent from the repeatability tests conducted during the test runs.

The heat transfer coefficient, $h=\frac{Q_{in}-Q_{loss}}{A(T_w-T_0)}$, was measured on the 9 x 12 cm^2 heat transfer surface, which consists of a 0.025 *mm* copper plate, a heating plate, and a balsa-wood insulation plate, see Fig. 2. Electrical power, Q_{in}, ranged from 6.3 to 40.6 watts with 3 percent uncertainty, was supplied to the heating plate from a *DC* power supply, resulting in a constant-heat-flux heat-transfer surface. The reference temperature, T_0, is the air inlet temperature, obtained using a Type-T, 0.1 *mm*-diameter thermocouple placed at the contraction section of the wind tunnel system. The surface temperature, T_w, distributions on the heat transfer surface were obtained using 99 thermocouples, where the junction beads of thermocouples were spot welded on the back of the copper plate. The surface temperatures were ranged from 56 ^oC to 94 ^oC under the investigated conditions with the uncertainty of 1^oC from repeatability tests. Heat conduction loss through the back of the heating plate is calculated using the Fourier's law, which is estimated to be less than 3 percent of the total heat generated. Radiation loss is estimated to be less than 3.6 percent of the total heat flux. Conduction loss along the sides of the heat transfer plate accounted for a small fraction and was neglected. The uncertainty in heat transfer measurement was estimated to be within 6 percent [12].

3. Results and Discussion

The cross-sectional flow structures in X-Z and X-Y planes for the flows without and with turbulator were discussed. Figure 3 presents a typical mean flow velocity vectors in the central (Y/H=0.5) X-Z plane for Re=15151 (U_d=5 m/s) without turbulator. In this central plane, the flow is subjected to no boundary-layer effect. Due to the side-opened, end-sealed duct geometry, the flow exhibits a free stagnation point flow behavior, where a positive pressure gradient exists in the direction of flow. The flow is forced to decelerate axially (X-direction) and accelerate transversely (Z-direction) outward as the flow approaches the end wall. A stagnation point essentially exists at X/L=1, Z/W=0. Similar flow structures were observed for other investigated Reynolds numbers. Figures 4(a-b) present the flow structures at Z/W=0.583 in X-Y plane without turbulator for Re=1546 (U_d=0.51 m/s) and 15151. In this cross-section, the flow is flowing in a duct where the end, top and bottom walls are sealed. Due to the end-sealed wall effect, the axial velocities decrease as the flow approaches the end wall. When the fluids impinge on the end wall, they are forced to flow upward and downward, and impinge on the top and bottom walls. Then, the fluids flow back to the main stream, causing the flow reversal and recirculation. Figure 4(a) shows that the flow is disturbed near the end wall and extended to the origin of test duct (X/L=0) for Re=1546. Reversed flow occurs approximately from X/L=0.38 to the end wall, and a small recirculation region occurs near the end wall. Figure 4(b) shows that the disturbed flow region for Re=15151 is smaller than that for Re=1546, due to the larger axial momentum and thinner boundary layer at the bottom wall. Reversed flow occurs approximately from X/L=0.78 to the end wall, and a recirculation region still occurs near the end wall. The flow structures at other Z/W positions are qualitatively similar to those shown in Figs. 4(a-b). The 45^o delta-wing turbulator effect on the flow structures in X-Y plane is presented in Figs. 5(a-d). It is noted that the turbulator, with vertical tip height of 0.7 cm (Y/H=0.233), is placed on the bottom wall upstream of the test duct (X/L=-0.3055). Apparently, the flows are largely disturbed by the turbulator, and much large reversed flow regions were observed. At Z/W=0, the fluid-blockage effect is the largest among other Z/W's. Figures 5(a) and 5(c) show that the investigated flows behave like flows over a backward-facing step, where the flow recirculation, reattachment and redevelopment occur. Flow recirculation regions occur downstream of the turbulator for both the investigated flows of Re=1546 and 15151. Larger recirculation regions occur for Re=1546 than Re=15151. As the flow impinges on the bottom wall, it redevelops and a second recirculation region occurs due to the end-sealed wall effect. The flow structures at Z/W=0.583 are qualitatively similar to those at Z/W=0. Since the fluid-blockage effect by the turbulator at Z/W=0.583 is not as large as that at Z/W=0, Figs. 5(b) and 5(d) show that the recirculation regions are smaller than those shown in Figs. 5(a) and 5(c).

The velocity fields in the boundary layers have major effects on the heat transfer process. Three near-wall flow parameters, including the convective mean velocity, secondary-flow velocity (i.e., the mean velocity normal to the heat transfer surface) and turbulent kinetic energy, were used to evaluate the relations between the local fluid flow and heat transfer [7]. Boundary-layer thickness measurements

showed that the boundary layer thicknesses for the investigated flows over the heat transfer surface were order of millimeters. Thus, three-component mean and fluctuating velocities at 2 mm from the heat transfer surface (bottom wall) were measured and the data were used to represent the near-wall flow characteristics.

The mean velocity parallel to the heat transfer surface is an indication of the convective effect on heat transfer. Its magnitude is expected to be proportional to the convective heat transfer rate. Figures 6(a-d) present the normalized near-wall convective mean velocity, $\sqrt{U^2+W_v^2}/U_d$, vectors for Re=1546 and 15151 without and with the 45^o delta-wing turbulator. In addition to the end-sealed wall effect, the fluids near the bottom wall are also subjected to the boundary-layer effect. The flow exhibits a retarded stagnation point flow behavior, where the flow is retarded by both the friction force and the positive pressure gradient. The flow decelerates axially and accelerates transversely outward as it approaches the end wall. The deceleration in the axial velocities is faster than that in free stagnation point flow and, eventually, the flow reversal occurs for both the investigated flows of Re=1546 and 15151. Figures 6(a-b) show that the flow reversal occurs earlier for Re=1546 than Re=15151 because of the smaller flow kinetic energy. The stagnation points roughly occur at X/L=0.4, Z/W=0 for Re=1546 and X/L=0.78, Z/W=0 for Re=15151. In the neighborhood of the stagnation points, the convective mean velocities are small and, thus, the heat transfer due to convective effect should also be small in these regions. The convective mean velocities are getting large from the stagnation points and, are large at duct side openings due to the flow accelerated transversely outward. The 45^o delta-wing turbulator effect on the convective mean velocity is shown in Figs. 6(c-d). The convective mean velocities are still large at duct side openings. Since the fluids are blocked by the turbulator, the convective mean velocities are small or negative behind the turbulator, as also discussed in Figs. 5(a-d). Also, the turbulator results in larger “dead water” flow regions, where the convective mean velocities are small. Thus, the turbulator may cause large regions of small heat transfer rate if the convective effect dominates the local heat transfer distribution.

Large strength of the secondary flow is expected to have a large effect on heat transfer. In this study, the Y-component mean velocity (V), perpendicular to the heat transfer surface, is used to represent to the secondary-flow effect [7]. According to the definition of the coordinate system in this study, the negative value of V indicates that the secondary flow is toward the heat transfer surface and tends to impinge and break the boundary layer. Thus, a large negative value of V has a better secondary-flow effect and should result in a large heat transfer rate. Figures 7(a-d) present distributions of near-wall normalized secondary-flow velocity, V/U_d, for Re=1546 and 15151 without and with the 45^o delta-wing turbulator. The vectors above and below dot lines represent positive and negative values of V/U_d, respectively. These figures indicate that the secondary-flow velocities are generally small except near the end wall, where large variations in the secondary-flow velocity occur. Large negative values of V/U_d occur at the measured X/L=0.944, and small or positive values of V/U_d occur at the measured X/L=0.889. These results are apparently related to the flow recirculation occurred near the end wall, as already shown in Fig. 4. Figures 7(a-b) also indicate that the flow secondary-flow effect is generally increased toward the duct side openings. The 45^o delta-wing turbulator effect on the secondary-flow velocity is presented in Figs. 7(c-d). The turbulator, in general, slightly increases the flow secondary-flow effect in most regions of the heat transfer surface. Also, the flow secondary-flow effect increases toward the duct side openings. Large variations in the secondary-flow velocity occur in the regions between the measured X/L=0.667 and X/L=0.944 due to the end- and bottom-wall effects, where the flow reversals occur as already discussed above. The heat transfer rates in these regions should be largely varied if the flow secondary-flow effect dominates the heat transfer distribution.

The turbulent kinetic energy, $(u'^2+v'^2+w'^2)/2$, was obtained from the X-, Y- and Z-component fluctuating velocities. Large turbulent kinetic energy is expected to have a large heat transfer rate. Figures 8(a-d) present distributions of near-wall normalized turbulent kinetic energy, $\sqrt{(u'^2+v'^2+w'^2)/2}/U_d$, for Re=1546 and 15151 without and with the 45^o delta-wing turbulator. The turbulent kinetic energy of the flows without the turbulator generally increases as the fluids flow downstream. The turbulator is expected to increase the flow turbulent kinetic energy. Figures 8(c-d) show that the increase in turbulent kinetic energy for Re=15151 is larger than that for Re=1546. In addition, the turbulator causes the turbulent kinetic energy more uniformly distributed on the heat transfer surface.

The heat transfer characteristics on the heat transfer surface are presented in a dimensionless form as a Nusselt number, $Nu=hD/k$, where k is the thermal conductivity of air, evaluated at the film temperature. Figures 9(a-f) present the local Nu distributions for three investigated Reynolds numbers without and with the 45^o delta-wing turbulator. It is shown in Figs. 9(a-c) that the Nu first decreases and, then, increases with X/L for the flows without turbulator. Also, the Nu increases toward the duct side openings. The location of minimum Nu depends on Reynolds number. It moves upstream toward the origin of test duct (X/L=0) as the Reynolds number increases. It is around X/L=0.4 for Re=1546, X/L=0.16 for Re=6121,

and near X/L=0 for Re=15151. These figures also show that the maximum Nu occurs near the end wall, duct side openings. The Nu distributions on the measured heat transfer surface are not largely varied, which is up to 50% for the investigated Reynolds numbers. The 45^o delta-wing turbulator effects on local Nu distributions are presented in Figs. 9(d-f), showing apparently different distributions from those without turbulator. The variation in local Nu is reduced, which is around 34.8% for Re=1546, 24% for Re=6121 and 12.6% for Re=15151. In addition, it is show in Fig. 9(d) that the location of minimum Nu moves further upstream to the origin of test duct for Re=1546. At, and large downstream regions from, the origin of test duct, the values of Nu are small. The Nu gradually increases as the fluids flow toward the end wall and duct side openings. On the contrary, Figs. 9(e-f) show that the values of Nu are large near the origin of test duct, slightly decrease and, then, increase with X/L. These local heat transfer characteristics are apparently related to the flow fields near the heat transfer surface, as discussed below.

In order to evaluate the turbulator effect on the overall heat transfer rate, the averaged Nusselt number, $\overline{Nu}$, on the heat transfer surface was computed by integrating the local Nusselt number, $\iint Nu(x,z)dxdz/A_1$, where $A_1 \cong A$. Since the insertion of turbulator into the flow causes an additional pressure loss compared with the flow without turbulator, these investigations were performed under a constant pumping power condition for a better comparison. In these measurements, the power input to the blower of the wind tunnel system for the flow with turbulator is equal to that for the flow without turbulator. The averaged Nusselt numbers for the general flows (i.e., the duct sides are sealed, and the duct end is open) of the investigated Reynolds numbers were also measured and compared. Figure 10 presents variations of $\overline{Nu}$ with Reynolds number for the general flows and present investigated flows without and with the 45^o delta-wing turbulator. The heat transfer rates in side-opened, end-sealed duct flows are apparently larger than those in general flows. This result is expected since the heat transfer is mainly by the convective effect in general flows, while it is by the flow secondary-flow and turbulence effects associated with the flow convective effect in a side-opened, end-sealed duct flow. Figure 10 also shows that the 45^o delta-wing turbulator augments the heat transfer rate for all of the investigated Reynolds numbers. The augmentation increases with Reynolds number, which is approximately 3.3% for Re=1546, and up to 35.3% for Re=15151. In view of the near-wall data shown in Figs. 6-8 and the results discussed above, the heat transfer augmentation is caused by the increases of the flow secondary-flow and, especially, the turbulence effects. Since the increase in flow turbulent kinetic energy is much larger for Re=15151 than that for Re=1546, the heat transfer augmentation by the turbulator is, accordingly, much larger for Re=15151 than Re=1546.

Comparing Figs. 6(a) and 9(a), Figs. 6(c) and 9(d), respectively, show a good similarity between the convective mean velocity and local Nusselt number distributions for Re=1546. Figure 6(a) shows that a minimum convective mean velocity occurs around X/L=0.4, Z/W=0. The convective mean velocities are getting large from this location and, are large at duct side openings. Figure 9(a) shows that the Nusselt number has a minimum value near X/L=0.4, Z/W=0, and increases from this location toward upstream, downstream and duct side openings. Also, Figure 6(c) shows that the turbulator causes negative and small connective velocities at, and large downstream regions from, the origin of test duct, where the values of Nusselt number are small, as presented in Fig. 9(d). These results suggest that the flow convective effect plays an important role in local heat transfer distribution for Re=1546. However, the convective mean velocity distributions are apparently different from the local Nusselt number distributions for Re=15151. Figure 6(b) shows that a minimum convective mean velocity occurs around X/L=0.8, Z/W=0. The convective mean velocities are getting large from this location and, are large at duct side openings. Figure 9(c) shows that the values of Nusselt number are small near the origin of test duct, and increase as the fluids flow downstream. Also, Fig. 6(d) shows that the convective mean velocities for the flow with turbulator are small at, and large downstream regions from, the origin of test duct. Figure 9(f) shows that the values of Nusselt number are large near the origin of test duct, decrease and, then, increase with X/L. These results suggest that the flow convective effect should not have a main effect on local Nusselt number distribution for Re=15151. It is also noted from Figs. 7(b) and 7(d) that the secondary flow velocities are largely varied near the end wall. Figures 9(c) and 9(f) show that the Nusselt number gradually varies near the end wall, suggesting that the flow secondary-flow effect should not play an important role in local Nusselt number distribution. Figures 8(b) and 9(c), respectively, show that the turbulent kinetic energy and Nusselt number increase as the fluids flow downstream. Figure 8(d) shows that the turbulator causes the increase of turbulent kinetic energy, which, in general, is large at the exit of test duct, slightly decrease and, then, increase with X/L up to X/L=0.78. This figure also shows that the variation in turbulent kinetic energy on the heat transfer surface is small. The Nusselt number distribution shown in Fig. 9(f) is generally similar to the turbulent kinetic energy distribution in most regions of the heat transfer surface. These results suggest that the flow turbulence effect has a profound effect on local Nusselt number distribution for Re=15151.

4. Conclusions

Several conclusions were drawn from the results of this research:

(1) Flow reversal and recirculation occur in the investigated duct flows. The turbulator causes large regions of flow reversal and flow recirculation, and results in the flow reattachment and redevelopment.

(2) The flow near the duct wall exhibits a retarded stagnation point flow behavior. The turbulator causes large regions of small convective mean velocities.

(3) The near-wall secondary-flow velocities are generally small except near the duct end wall, where large variations in the secondary-flow velocity occur. The turbulator generally slightly increases the flow secondary-flow effect.

(4) The near-wall flow turbulent kinetic energy, in general, increases as the fluids flow downstream. The turbulator increases the flow turbulent kinetic energy, and causes the turbulent kinetic energy more uniformly distributed on the heat transfer surface.

(5) The maximum Nu, in general, occurs near the duct end wall, duct side openings. The location of minimum Nu depends on Reynolds number. It moves upstream toward the origin of test duct (X/L=0) as the Reynolds number increases. The turbulator causes small heat transfer rates at, and large regions from, the origin of test duct for Re=1546. On the contrary, large heat transfer rates occur near the origin of test duct for all of other investigated Reynolds numbers.

(6) The turbulator augments the heat transfer rate, and the augmentation increases with Reynolds number. The heat transfer augmentation is mainly caused by the increases of the flow secondary-flow and, especially, the turbulence effects.

(7) The flow convective effect plays an important role in local heat transfer distribution for Re=1546, while the flow turbulence effect has a profound effect on local heat transfer distribution for Re=15151.

References

1. P. A. Eibeck, J. K. Eaton, Heat transfer effects of a longitudinal vortex embedded in a turbulent boundary layer, Journal of Heat Transfer, 109 (1987) 16-24.
2. M. Fiebig, P. Kallweit, N. Mitra, S. Tiggelbeck, Heat transfer enhancement and drag by longitudinal vortex generators in channel flow, Experimental Thermal and Fluid Science, 4 (1991) 103-114.
3. S. Tiggelbeck, N. Mitra, M. Fiebig, Flow structure and heat transfer in a channel with multiple longitudinal vortex generators, Experimental Thermal and Fluid Science, 5 (1992) 425-436.
4. S. Tiggelbeck, N. Mitra, M. Fiebig, Comparison of wing-type vortex generators for heat transfer enhancement in channel flows, Journal of Heat Transfer, 116 (1994) 880-885.
5. J. P. Tsia, J. J. Hwang, Measurements of heat transfer and fluid flow in a rectangular duct with alternate attached-detached rib-arrays, International Journal of Heat and Mass Transfer, 42 (1999) 2071-2083.
6. T. M. Liou, J. J. Hwang, Effect of ridge shapes on turbulent heat transfer and friction in a rectangular channel, International Journal of Heat and Mass Transfer, 36 (4) (1993) 931-940.
7. T. M. Liou, C. C. Chen; Y. Y. Tzeng, T. W. Tsai, Non-intrusive measurements of near-wall fluid flow and surface heat transfer in a serpentine passage, International Journal of Heat Mass Transfer 43 (2000) 3233-3244.
8. T. Y. Chen and H. T. Shu, Flow structures and heat transfer characteristics in fan-flows with and without delta-wing vortex generator, Experimental Thermal and Fluid Science, 28(4) (2004), pp.273-282.
9. T. Y. Chen and Y. H. Chen, Rectangular-plate turbulator effects on heat transfer and near-wall flow characteristics in fan flows, Journal of Mechanics, 20 (1) (2004), pp. 33-41.
10. S.W. Chnag, L. M. Su, T. L. Yang and S. F. Chiou, Enhanced heat transfer of forced convective fin flow with transverse ribs, International Journal of Thermal Science, 43(2004), pp. 185-200.
11. K. F. Chiang, S. W. Chnag and P. H. Chen, Forced convective heat transfer of 45^{o} rib-roughened fin flows, Experimental Thermal and Fluids Science, 29 (2005), pp. 743-754.
12. Editorial Board of ASME Journal of Heat Transfer, Journal of heat transfer policy on reporting uncertainties in experiments and results. ASME Journal of Heat Transfer 115 (1993), pp. 5-6.

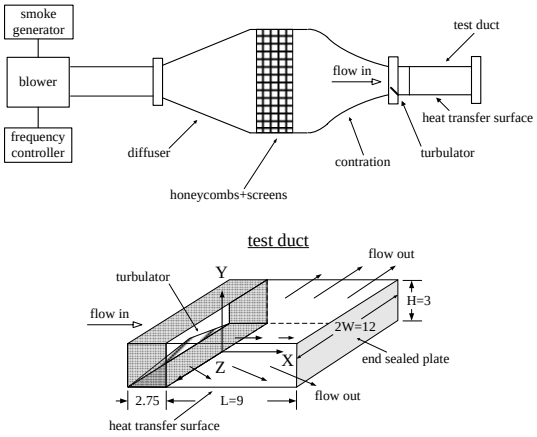

Figure 1: A schematic of the experimental setup (unit: cm).

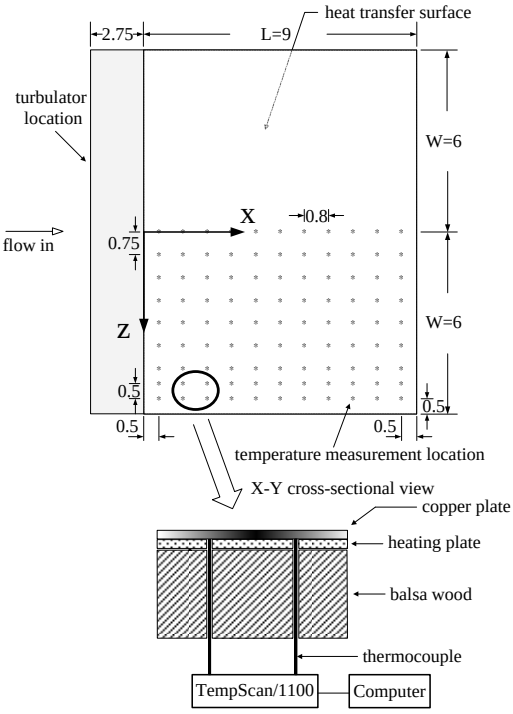

Figure 2: The temperature measurement locations, and a sketch of the heat transfer surface (unit: cm).

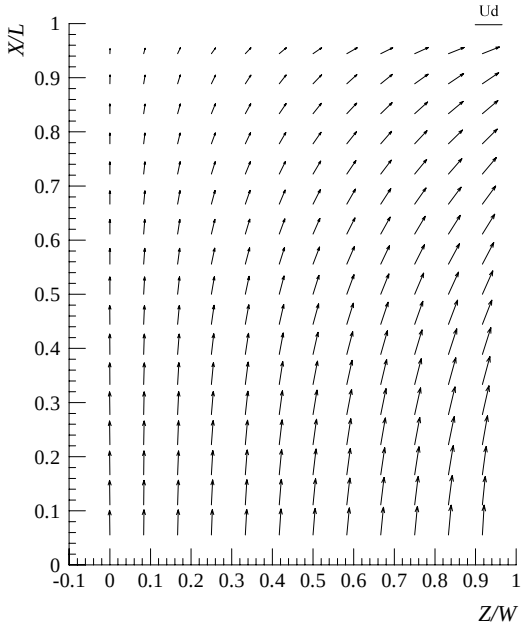

Figure 3: The mean flow velocity vectors in the central (Y/H=0.5) X-Z plane without turbulator for Re=15151.

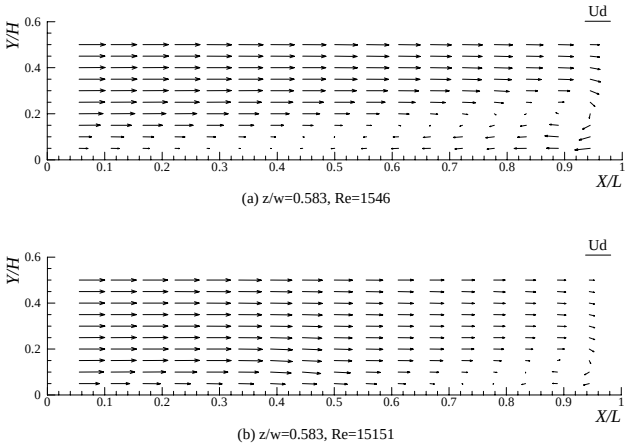

Figure 4: The mean flow velocity vectors in X-Y plane without turbulator for Re=1546 and 15151.

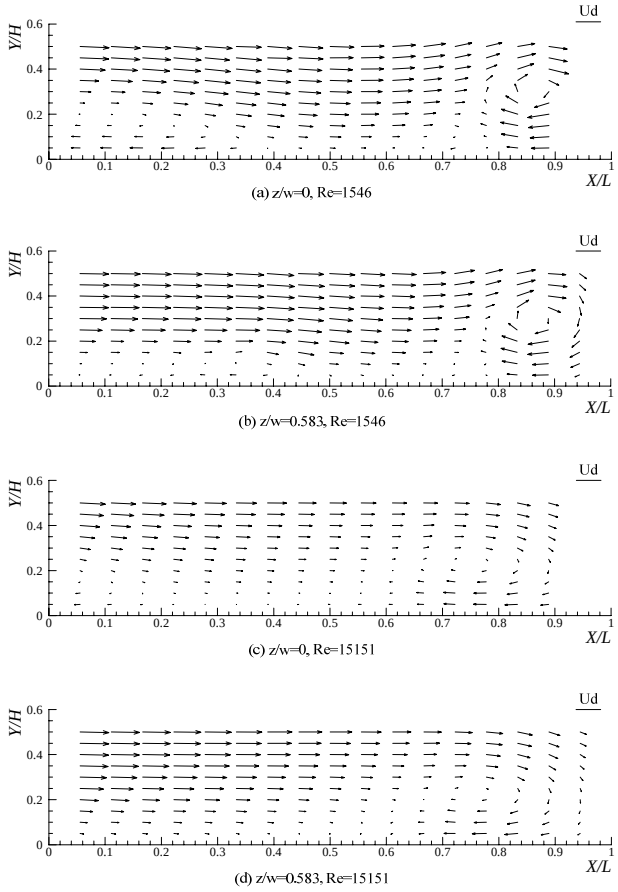

Figure 5: The mean flow velocity vectors in X-Y plane with 45° delta-wing turbulator for Re=1546 and 15151.

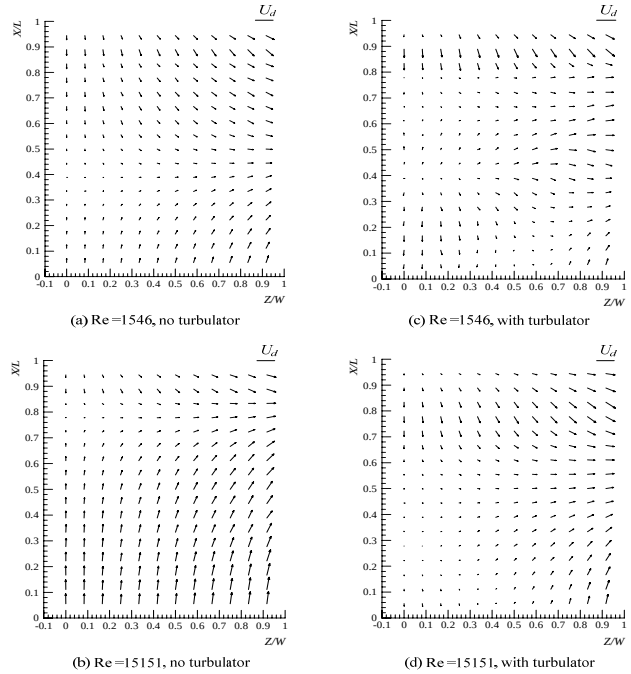

Figure 6: Near-wall convective mean velocity vectors for Re=1546 and 15151 without and with 45° delta-wing turbulator.

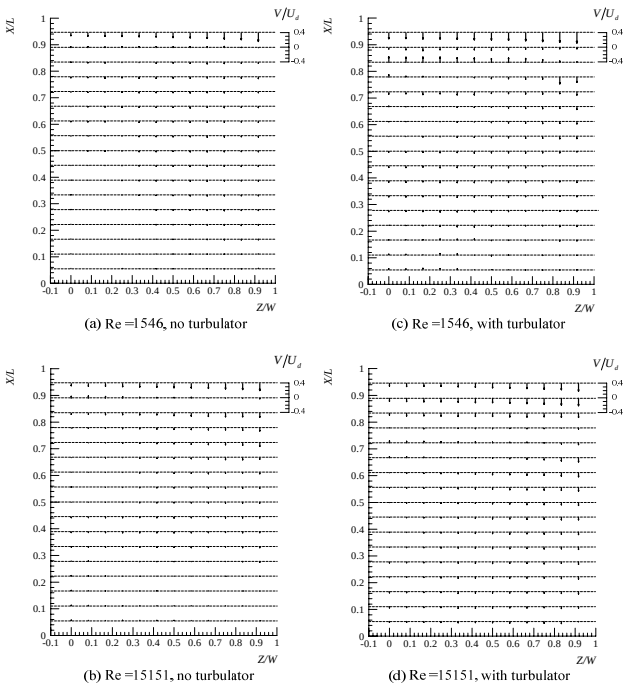

Figure 7: Distributions of near-wall normalized secondary flow velocity, V/U_d , for Re=1546 and 15151 without and with 45° delta-wing turbulator.

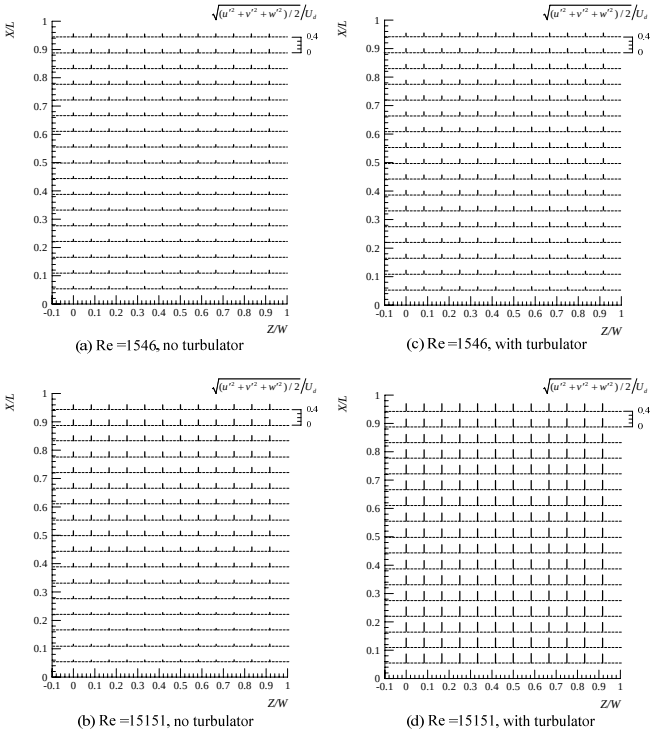

Figure 8: Distributions of near-wall normalized turbulent kinetic energy for Re=1546 and 15151 without and with 45° delta-wing turbulator.

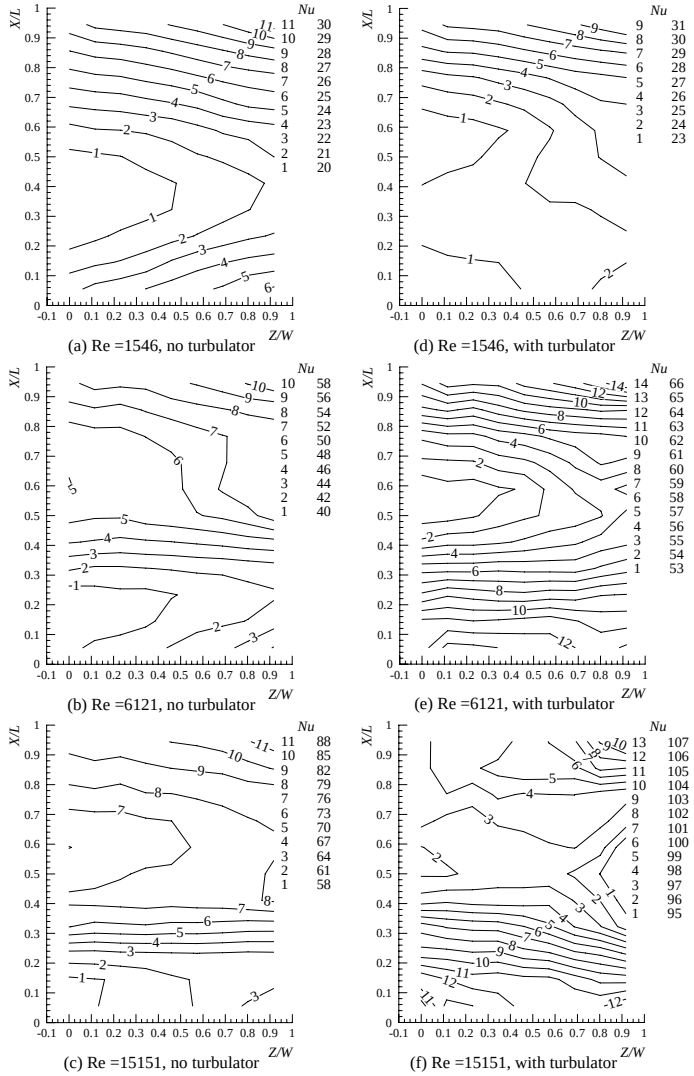

Figure 9: Local Nusselt number distributions for Re=1546, 6121 and 15151 without and with 45° delta-wing turbulator.

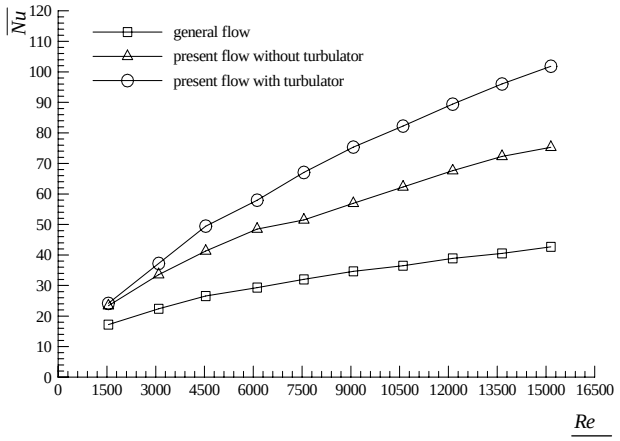

Figure 10: Variations of averaged Nusselt number, $\frac{\overline{Nu}}{Nu}$, with Reynolds number without and with 45° delta-wing turbulator.